

Quantum Effects or Theoretical Artifacts? A Computational Reanalysis of Hydrogen at High-Pressure

Stefano Racioppi,^{1,2} Eva Zurek¹

¹Department of Chemistry, State University of New York at Buffalo, Buffalo, New York 14260-3000, USA.

²Department of Materials Science and Metallurgy, University of Cambridge, Cambridge CB30FS, United Kingdom.

Abstract

The stability of high-pressure phases of hydrogen remains a central question in condensed matter physics, where both experimental observations and theoretical predictions are highly sensitive to methodological choices. Here, we revisit the cold phase diagram of hydrogen between 400 and 700 GPa using the meta-GGA functionals (R²SCAN and SCAN0) and compare the results with the more common PBE. At the meta-GGA level, molecular phases (*Cmca-4*, *Cmca-12*, and *C2/c*) are stabilized over the atomic *I4₁/amd* phase up to significantly higher pressures than predicted by GGA, in closer agreement with diffusion Monte Carlo calculations and experimental observations of band-gap closure near 425 GPa. Furthermore, phonon spectra calculated with R²SCAN show that the dynamical instabilities and anharmonic signatures previously predicted at the GGA level vanish, indicating that such effects may partly arise from functional deficiencies rather than genuine nuclear quantum effects. Bonding analysis reveals that PBE artificially weakens intramolecular H–H bonds and enhances intermolecular interactions through charge delocalization, whereas meta-GGA preserves a more localized molecular character. Anharmonic motion remains relevant for finite-temperature dynamics; however, we demonstrate that the accurate description of the potential energy surface—particularly its curvature near equilibrium—is pivotal for assessing both phase stability and bonding of hydrogen at high-pressure.

Almost a hundred years after Wigner and Huntington estimated that hydrogen, the most abundant element in the Universe, would become a metallic solid at 25 GPa of pressure,¹ the existence of this exotic phase is still under debate.^{2,3} Even with the technology in hand to reach pressures almost two orders of magnitude higher than that initially predicted, hydrogen metallization in the solid state⁴ remains elusive up to 500 GPa.^{5,6} Chasing metallic hydrogen has surely boosted an incredible development of modern high-pressure (HP) experiment techniques.⁷ Yet, the crystal structure of hydrogen at 212 GPa was solved only recently,⁸ resulting in a post-*hcp* structure that has never been predicted in decades of computations. In fact, theory struggles behind and keeps being challenged by the small atom. Within Density Functional Theory (DFT), the workhorse of numerical quantum chemistry, computations involving hydrogen are plagued by a series of phenomena arising from the use of non-exact functionals of the electron density,⁹ causing the artificial interaction of the single electron with itself, and wrecking the quantum mechanical interpretation. Specifically, the delocalization and static correlation errors,¹⁰ together with the incorrect asymptotic behavior of the exchange-correlation potentials,¹¹ are the main limitations. These errors, also related with the lack of a physical interpretation of the Kohn-Sham (KS) orbitals,¹² are unfortunately amplified in the case hydrogen. Considering an isolated H atom, the binding energy calculated one of the most used Generalized Gradient Approximation (GGA) functional, PBE,¹³ can be as off as 50% compared to the experimental value (13.6 eV), caused by estimations of electron-electron interactions, in the mono-electronic system, of the order of 5–7 eV.¹⁴

Nonetheless, there is still margin of improvement, especially from the use of alternative semi-local functionals. The exchange-correlation energy is one of the main components contributing to glue atoms together.¹⁵ Meta-GGA functionals¹⁶ bring a substantial improvement over GGAs by employing the kinetic energy density to check the correct behavior of the correlation energy, as well as by approaching the correct gradient expansions in the exchange and correlation energies for slowly varying densities (*i.e.*, metals).^{17,18} As a consequence, meta-GGA functionals calculates better band-gaps (which is severely underestimated by GGAs functionals) and bonding properties.^{19,20} Alternative, but computationally more expensive,

methods exist to correctly evaluate the electronic structure of hydrogen, such as Quantum Monte Carlo (QMC)²¹ and coupled-cluster.²² Yet, some meta-GGA functionals can substantially improve the outcome of electronic structure calculations, at almost GGA computational cost.²³

Therefore, we decided to take another look at the cold (0 K) HP phase diagram of hydrogen between 400 and 700 GPa using the meta-GGA functional R²SCAN²⁴ (first part of the paper) and reanalyze the quantum mechanical contribution to the stability of some critical structures (second part of the paper). Specifically, we focused on the molecular phases *Cmca-12*²⁵ and *Cmca-4*²⁶ (12 and 4 refers to the number of atoms in the primitive unit cell, even if conventional unit cells were used through this work), which stabilities were proposed to be governed by anharmonic effects,^{27,28} and on the elusive atomic phase *I4₁/amd*,²⁵ characterized by a Cs-IV type of structure.²⁹ We also considered the C2/c phase (phase-III),²⁵ which might still be relatively competitive at those pressures (Figure S1).

First of all, the presence of additional phases of hydrogen at 500 GPa was checked using the evolutionary algorithm-based crystal structure prediction code XtalOpt, checking units cells having up to 32 atoms, and using the meta-GGA functional R²SCAN-L.²³ The search found no new (meta)stable phases which could be competitive to the other known high-pressure phases.

The 0 K phase diagram of hydrogen was then calculated between 400 GPa and 700 GPa, with 100 GPa steps, at three different levels of theory – PBE, R²SCAN and SCAN0 – to highlight the impact of the exchange-correlation functional on the phases' stabilizations (Figure 1). At the GGA level (PBE), we predict that the atomic phase *I4₁/amd* has lower energy than *Cmca-4* at approximately 507 GPa. All calculated phases, including *Cmca-12* and C2/c, are metallic at this level or theory. The *Cmca-4* → *I4₁/amd* phase transition results comparable with previous calculations performed with the same functional, but different code (Quantum Espresso), which was predicted at 490 GPa.⁴ Previous diffusion quantum Monte Carlo (DCM) calculations,³⁰ instead, predicted that *I4₁/amd* becomes the ground state phase at 374 GPa. To be noted, because of the fixed-node approximation³¹ used by DCM, these calculations relied on the local density approximation (LDA) to calculate the orbitals energies and geometries, which inevitably affects the final result of the Monte Carlo simulation and can be a substantial source of error.³²

Moving now to the meta-GGA level, R²SCAN predicts that the *Cmca-4* phase is the ground state over *Cmca-12* only above 430 GPa and up to 675 GPa, before transforming into the atomic *I4₁/amd* phase (Figure 1). Also in this case, the low energy phases have zero band gaps. However, the C2/c phase, which is just a couple of meV/atom less stable than the ground states (Figure S1), possess a band gap of 0.41 eV at 400 GPa, that closes before 500 GPa. Interestingly, spectroscopic experiments showed that a phase transition, sided by a band gap closure, occurs at ~425 GPa.⁵ A more recent series of DMC calculations, now based on the PBE geometries and energies, instead of LDA,³³ predicted a similar transition from the *Cmca-12* in this regime of pressure (447 GPa), but to the atomic phase, and not to *Cmca-4*.

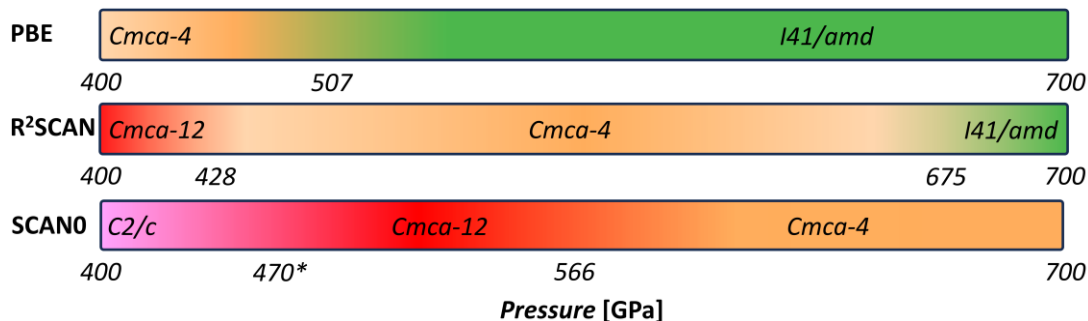


Figure 1. Three cold (0 K) phase diagrams ($\Delta H = \Delta E + P\Delta V$) of HP hydrogen, using: (1) the PBE GGA functional; (2) the R²SCAN meta-GGA functional; and (3) the SCAN0 meta-hybrid-GGA functional. The SCAN0 energies were calculated on the geometries optimized with R²SCAN. At 470 (*), the phase transition predicted by SCAN0 is sided by the band-gap closure (experimentally, a band gap closure was observed at ~425 GPa).⁵

Is it possible to go beyond meta-GGA? In principle, using meta-hybrid, double-hybrid and higher level functional would be ideal to study hydrogen, since the inclusion of Hartree-Fock to exactly calculate the exchange energy has a great impact on the evaluation of the electronic energy and structures of compounds based on the first element of the periodic table.¹⁰ Unfortunately, using such high level of theory in periodic systems is hindered by the huge computational cost required to calculate the exact exchange with plane-wave based codes. Therefore, to date, performing geometry optimizations and phonons to study the high-pressure phases of hydrogen with hybrid levels of theory is mostly prohibited. However, we attempted calculations of the single point energies of *C2/c*, *I4₁/amd*, *Cmca-4* and *Cmca-12* from 400 to 700 GPa using the meta-hybrid GGA functional SCAN0 on the R²SCAN optimized geometries (Figure 1).³⁴ The forces estimated by the SCAN0 single point calculations were all below 10⁻¹³ eV/Å, suggesting that the molecular and atomic phases of hydrogen would not change much upon re-optimization at the meta-hybrid GGA level. On the other hand, the SCAN0 energies change compared to the previous cases. The most striking result emerging from this estimate is that at 400 GPa, the *C2/c* phase is now the ground state with a band gap of 1.75 eV. We calculate that this band gap lowers to 0.79 eV at 500 GPa, before closing at higher pressures. However, we predict a phase transition to the *Cmca-12* phase at around 470 GPa, also sided by the closure of the band gap (even at SCAN0 level of theory; only the *C2/c* phase is predicted to possess a band gap). This insulator-to-metal transition is now in agreement with the infrared observations done at 80 K by Loubeire and coworkers (transition observed above 425 GPa).⁵ By increasing the pressure, a second transition is predicted, transforming *Cmca-12* into *Cmca-4* at ~566 GPa, which then remains the most stable phase up to the limit of our calculations (700 GPa). By extrapolation of the meta-hybrid GGA enthalpies, the stabilization of the atomic *I4₁/amd* phase is estimated above 850 GPa, which is way beyond any experiment performed thus far on hydrogen.

With this first section, we aimed to highlight the sensitivity of the predicted phase diagram of hydrogen to the level of theory in the context of DFT. As consequence, it is also not possible to exclude that similar effects would be observed while modeling exotic states of matter based on hydrogen interaction, such as superionicity,³⁵ or the formation of superconducting hydrogen cages in superhydrides.³⁶ Moreover, we observed that by increasing the level of theory through the exploration of the static (0 K) phase diagram, the atomic phase *I4₁/amd* is pushed more and more towards higher pressures, favoring and stabilizing the molecular phases thanks to a better evaluation of the kinetic and exchange-correlation energy.

Moving to the second part of this work, we want to compare our results with previous DFT works and highlight how different functionals, specifically GGA and meta-GGA, can impact the modelling of the potential energy surface and the physical interpretation of quantum effects and chemical bonding in HP molecular and atomic hydrogen.

Previous calculations at the BLYP level of theory,^{28,37} where anharmonic effects were included, predicted *Cmca-12* as the ground state phase of hydrogen, before transforming into the atomic phase at 577 GPa,²⁵ without passing through the *Cmca-4* phase. In fact, other works done with the PBE functional then predicted that the *Cmca-4* phase becomes dynamically unstable at 450 GPa.^{27,38} However, the unstable phonons could be renormalized by anharmonic effects calculated with the stochastic self-consistent harmonic approximation (SSCHA).^{27,38}

Our calculations give, instead, a different picture. In particular, the meta-GGA functional R²SCAN does not calculate imaginary phonons for *Cmca-4* in the range of pressure considered (Figure 2), contrary to the GGA functionals. We will try to understand the origin for these discrepancies, particularly by checking whether the use of functionals that are not designed to capture important interactions in hydrogen-based compounds can affect properties arising from the shape of the potential energy surface (PES).

We now proceed by showing the harmonic phonon spectra calculated for the four phases at 700 GPa optimized using either the PBE or the R²SCAN functionals (Figure 2a-d). Firstly, for the atomic phase (Figure 2a), the phonon bands calculated with the two functionals do not show striking differences, apart from a hardening of the phonon modes along $\Gamma \rightarrow X$ and at N with the meta-GGA functional. This effect is opposite to what calculated in previous work including anharmonic effects, which, instead, produced even softer phonons at these symmetry points.³⁹ Those calculations were, however, done at 500 GPa, and therefore closer to the phase transition's pressure predicted by PBE. Yet, the phonon renormalization and the atomic volume expansion caused by the anharmonic effects were quite mild. In fact, the *I4₁/amd* was already predicted to be highly harmonic.^{28,37} The meta-GGA functional calculates as well slightly larger

volume per atom in *I4₁/amd* compared to GGA, especially at lower pressures (Figure S2), but the effect on the phonons is not as evident as for the molecular phases (see below).

However, we are not the first to notice that the PES of *I4₁/amd* can be adequately calculated even by lower level functionals. In Ref ²⁸, it is reported (in the supporting Information) a comparison of the calculated energy variation of *I4₁/amd* in function of the *c/a* ratio between LDA, GGA and QMC. Surprisingly, for small atomic volumes (*i.e.*, high pressures) LDA and GGA predict energy profiles that almost match that of QMC. This is likely due to the transition from covalent molecule (localized electron pair) to atomic metal (free electron gas-like), which can be fairly described also by the LDA approximation.

The two *Cmca* and the *C2/c* molecular phases are, instead, the most affected by the change of the functional. Within the harmonic approximations, GGA functionals like PBE (Figure 2b) or BLYP^{27,28} calculate that *Cmca-4* is dynamically unstable at 700 GPa. At the BLYP level of theory, the instability arises already at ~400 GPa.²⁷ On the other hand, the meta-GGA functional, predicts neither dynamic instabilities nor soft phonon modes that could be signature of anharmonicity (Figure 2b). As we will discuss later, this difference boils down to the ability of meta-GGA to better calculate intra and intermolecular hydrogen interactions, which are at the core of the phonon dispersions. A similar hardening of the phonons is evident both in *Cmca-12* and in *C2/c* once the meta-GGA functional is used (Figure 2c-d), despite PBE does not calculate dynamic instabilities in the former case. Interestingly, R²SCAN calculates a volumes expansion for all the phases, resembling that predicted by the introduction of anharmonic effects (Figure S2).²⁷

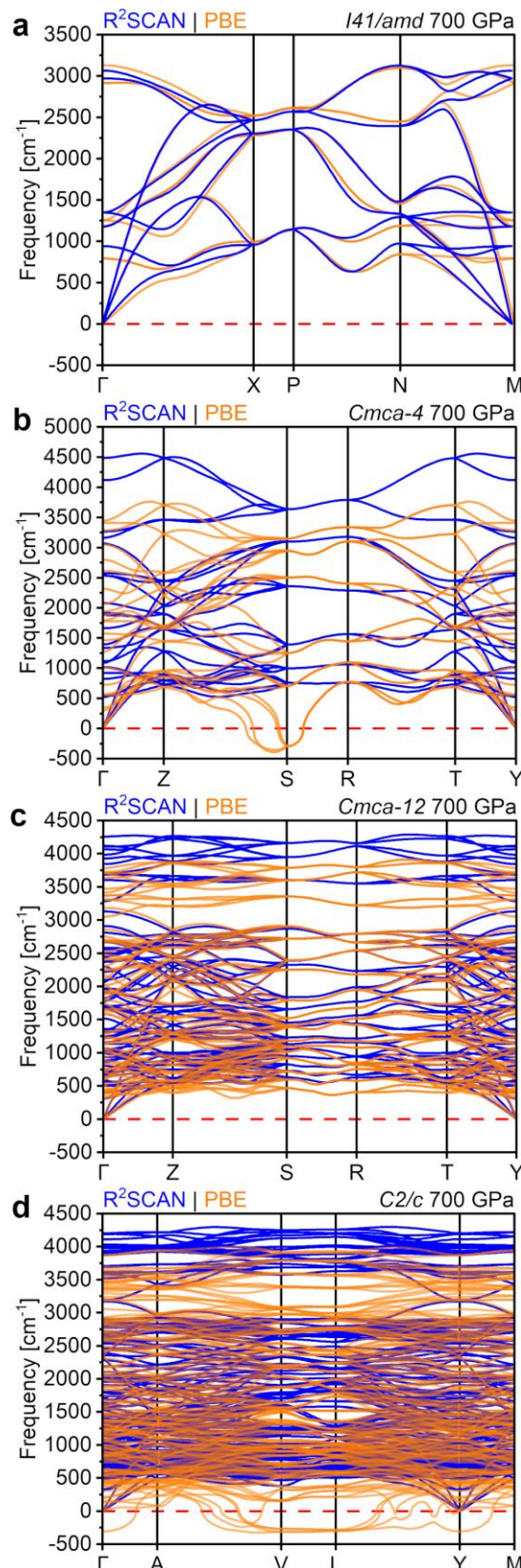


Figure 2. Phonon band structures of the optimized *I4₁/amd*, *Cmca-4*, *Cmca-12* and *C2/c* phases, calculated at $P = 700$ GPa with VASP using both the PBE (orange lines) and the R²SCAN (blue lines) functionals.

However, in the case of the meta-GGA functional, the reason for the expansion is not due to elongations of the H-H interactions, as instead predicted by the SSCHA,²⁷ but to the increase of the Pauli repulsion between molecules (see below). The crucial effect of explicitly introducing the dependence on $\nabla^2\rho$ in the functional to calculate the PES of molecular HP hydrogen becomes even more evident in quantum molecular dynamic calculations (Figure S3). Performing *NPT* simulations on the *Cmca-4* phase at 700 GPa and 300 K, the PBE functional calculates the system as unstable, in agreement with the imaginary modes calculate in the phonon spectra (Figure 2b). On the other hand, the meta-GGA functional holds the crystallinity of the system even at room temperature (Figure S3).

To better quantify these differences between functionals, let's shift the attention on the way that GGA and meta-GGA predict the intramolecular interactions in molecular hydrogen (Figure 3). By relaxing the orthorhombic unit cell and the atomic positions of *Cmca-4* at 700 GPa, that we use here as general example, the intramolecular H-H distance is calculated equal to 0.836 Å and 0.752 Å for PBE and R²SCAN respectively. If we then rigidly extract a molecular unit of H₂ from the unit cell (therefore without further relaxations), and calculate the difference between the lowest unoccupied molecular orbital (LUMO) and the highest occupied molecular orbital (HOMO), the band gaps associated with PBE and R²SCAN are equal to 9.73 eV and 10.98 eV. Scanning then the energy profile under pressure of the extracted H₂ molecules in function of the H-H distance, as shown in Figure 3, we observe that the molecule of hydrogen calculated by meta-GGA is already near its minimum. In other words, for R²SCAN, the *Cmca-4* phase is a pure molecular crystal. In fact, by re-optimizing the geometry of the isolated molecule under pressure, the H-H bond shortens by only 0.01 Å, and the band gap (HOMO – LUMO difference) lowers by less than 0.1 eV (Figure 3).

On the other hand, the energy profile calculated with PBE reveals that the extracted hydrogen molecule is not at its minimum of energy. This means that at the GGA level, the molecular nature of H₂ in the *Cmca-4* crystal is perturbed. In fact, PBE weakens the H₂ bond when the molecule is embedded in the *Cmca-4* crystal lattice, resulting in an elongation of H-H bond by almost 0.1 Å. This is due to the fact that GGA functionals like PBE tend to over delocalize the electron density, producing periodic systems that are more metallic, and causing also the famous under estimation of the band gaps. Instead, by relaxing the isolated molecules under pressure with the same functional, and therefore removing the possibility of diffusing the electron density over the adjacent molecules, the H-H distance contracts to 0.750 Å, and the HOMO – LUMO increase to 10.15 eV, which is in line with the molecular behavior calculated by R²SCAN.

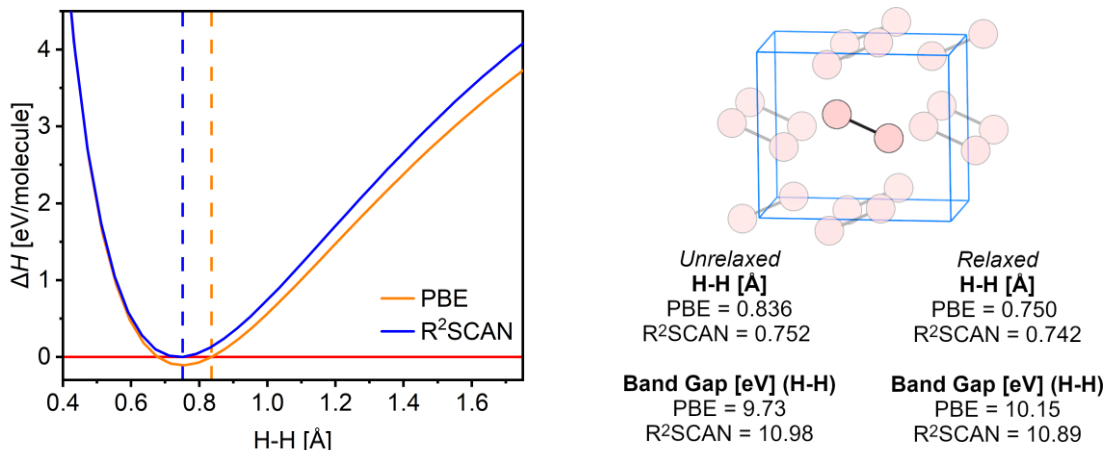


Figure 3. On the left, the energy profiles of H₂ in function of the intermolecular distance, calculated with R²SCAN and PBE under pressure. Dashed lines locate the molecular H-H distances in the *Cmca-4* crystal structure as calculated by the two functionals. The zero line is set at the energy of the H₂ molecules as extracted from the crystal (unrelaxed). On the right, the interatomic distance and band gap (HOMO – LUMO gap) of the: unrelaxed hydrogen molecule as extracted from the crystalline environment of *Cmca-4* at 700 GPa, and the “isolated” hydrogen molecule, relaxed at the same pressure conditions.

The effects of electron density delocalization calculated by PBE in *Cmca-4* can be further quantified by mean of Quantum Theory of Atoms in Molecules (QTAIM, See Figure S4). In this context, the value of the electron density $\rho(\mathbf{r})$ at the intramolecular bond critical point $\text{bcp}(1)$ (See Supporting Information for further details), becomes a useful descriptor to benchmark the effect of the functional on the bond strength of HP molecular hydrogen, while the value of the Laplacian, $\nabla^2\rho(\mathbf{r})$, quantify the degree of localization of the electron density at the bonding critical point. The values of $\rho(\mathbf{r})$ and $\nabla^2\rho(\mathbf{r})$ calculated using the PBE functional are much lower, and way more diffused than those calculated with R²SCAN, demonstrating that the GGA functional tends to produce weaker H-H bonds. However, PBE counterbalances this weakening of the H₂ molecular bonds by delocalizing the charge density through the adjacent molecules and strengthening, instead, the intermolecular interactions ($\text{bcp}(2)$ and $\text{bcp}(3)$, Figure S4). This phenomenon directly affects also the density of states at the Fermi level (Figure S5), which in the case of PBE, are almost 30% higher than in R²SCAN. This marked difference in the electronic structure and electron density calculated by GGA and meta-GGA functionals is not observed in the atomic phase *I4₁/amd*, which instead, is well described by both functionals as a metallic atomic polymer (Figure S4-S5).

To conclude the bonding analysis, we used the Periodic Energy Decomposition Analysis (PEDA, see also the Supporting Information for further explanation)⁴⁰ to decompose the different terms of the intermolecular interaction energy between a hydrogen molecule and its surrounding in *Cmca-4*, as electrostatic (ionic), orbital (covalent) and Pauli repulsion contributions (Figure S6). The energy decomposition was calculated in three different scenarios: (1) from the PBE energy calculated in the PBE relaxed structure; (2) from the R²SCAN energy calculated in the PBE relaxed structure; and (3) from the R²SCAN energy calculated in the R²SCAN relaxed structure.

The energy difference between (1) and (2) is purely given by the different functionals, since the unit cell and the atomic positions are the same. In this comparison, R²SCAN calculates weaker interactions between the reference H₂ molecule and the rest of the surrounding crystal. The higher Pauli repulsion in (2) and lower orbital interaction with the adjacent hydrogen molecules, are the main responsible terms for this effect, since with meta-GGA functional, the charge is less delocalized between molecules, but more concentrated in the H₂ intramolecular bond (Figure S5). In fact, in the scenario (3), where the unit cell and atomic coordinates are optimized using the same meta-GGA functional, the H₂ intramolecular distance shortens, while the unit volume expands. In energy terms, this is translated as a drop of the Pauli repulsion between molecules, but also a lowering of the intermolecular interactions. Therefore, the volume expansion in *Cmca-4* calculated by R²SCAN is the way that the system adopts to lower the intermolecular Pauli repulsion.

In conclusion, we analyzed the effect of GGA, meta-GGA and meta-hybrid GGA functionals on the thermodynamic stability and bonding character of hydrogen phases at high-pressure. We showed that the phonon instabilities calculated for some of the molecular phases of hydrogen (*Cmca-4*, *Cmca-12* and *C2/c*) at the GGA level of theory, disappear when the potential energy surface is computed using a meta-GGA functional such as R²SCAN. Meta-GGA functionals improve the evaluation of quantum mechanical energy terms that are critical for the correct description of the electronic structure and bonding character of hydrogen, showing that molecular phases can retain a substantial harmonic character also at high-pressure. We pointed out that modelling the correct shape and the curvature of the potential energy surface using functionals appropriate for the nature of the system is a crucial step for the evaluation of the dynamic behaviors and bonding properties.

Methods

Crystal Structure Prediction

The open-source evolutionary algorithm XtalOpt^{41,42} version 13.0 was employed for crystal structure prediction (CSP). Two crystal structures predictions were performed at 500 GPa. The initial generation consisted of 300 random symmetric structures that were created by the RandSpg algorithm.⁴³ The number of formula units (FUs) for the stoichiometry H was set up to 32. Duplicate structures were identified and removed from the breeding pool using the XtalComp algorithm.⁴⁴ The total number of generated structures was equal to 2000. Each structure search followed a multi-step strategy, with three subsequent optimizations with increased level of accuracy, followed by a final accurate single. Geometry optimizations and electronic structure calculations were performed using Density Functional Theory (DFT) with the

Vienna Ab Initio Simulation Package (VASP), version 6.4.2.⁴⁵ The meta-GGA R²SCAN-L²³ exchange-correlation functional was employed. The projector augmented wave (PAW) method⁴⁶ was used to treat the core states in combination with a plane-wave basis set with an energy cutoff of 600 eV for the geometry optimizations. The non-spherical contributions related to the gradient of the density in the PAW spheres was included. The k -point meshes were generated using the Γ -centered Monkhorst–Pack scheme,⁴⁷ and the number of divisions along each reciprocal lattice vector was selected so that the product of this number with the real lattice constant was greater than or equal to 60 Å. The accuracy of the energy convergence was set to increase from 10^{-5} eV, for which the norms of all the forces calculated during the relaxations were smaller than 10^{-3} eV/Å. A Gaussian smearing was used at each optimization step, and for each system with a sigma of 0.02 eV.

Electronic Structure and Topology

We performed periodic Density Functional Theory (DFT) calculations using VASP, version 6.4.2.⁴⁵ The R²SCAN²⁴ and PBE¹³ exchange-correlation functional were employed for the geometry optimizations and calculations of the electronic properties of the known structures of hydrogen and those found by XtalOpt. The projected augmented wave (PAW) method,⁴⁶ with a cutoff of 700 eV. The k -point meshes were generated using the Γ -centered Monkhorst–Pack scheme,⁴⁷ and the number of divisions along each reciprocal lattice vector was selected so that the product of this number with the real lattice constant was greater than or equal to 60 Å. For the geometry optimizations, the accuracy of the energy convergence was set to 10^{-6} eV and the norms of all the forces calculated during the relaxations were smaller than 10^{-3} (eV/Å). The Methfessel-Paxton smearing method was adopted in the geometry optimizations of the metallic phases,⁴⁸ while the tetrahedron smearing method was used to calculate the electronic properties on the optimized geometries.⁴⁹ The non-spherical contributions related to the gradient of the density in the PAW spheres was included. For the projected density of states, the Wigner-Seitz radius of H was recalculated for each phase and at each pressure point form the volume of the unit cells. The topological analysis of the electron density, based on the Quantum Theory of Atoms in Molecules (QTAIM),⁵⁰ was performed using the Critic2 code.⁵¹ Phonons in the harmonic approximation were determined with the Phonopy package⁵² using supercells equal to 3x2x3 *Cmca-12*, 4x3x3 for *Cmca-4* and 4x4x2 for *I4/amd*, based on the conventional unit cells of the R²SCAN optimized structures. A finite displacement of 0.003 Å was used, and accuracy of the energy convergence was set to 10^{-8} eV. Single point energies were also calculated at the meta-hybrid GGA level of theory with the SCAN0³⁴ functional on the R²SCAN optimized geometries maintaining the same computational parameters of accuracy, cutoff, smearing (tetrahedron) and k -point mesh.

Molecular Dynamics

Molecular dynamics using isothermal-isobaric (NPT) ensemble and the Langevin thermostat^{53,54} at $T = 300$ K (a Fermi smearing was employed) and at $P = 700$ GPa was performed for *Cmca-4* using both the functionals the PBE and the R²SCAN functionals on a 4x3x3 supercells (288 atoms). The duration of the simulation was set to 5 ps with 1 fs time steps. The projected augmented wave (PAW) method,⁴⁶ with a cutoff of 700 eV was used and the accuracy of the energy convergence was set to 10^{-5} eV.

Energy Decomposition Analysis

To evaluate the energy interaction terms within periodic energy decomposition analysis (PEDA),⁴⁰ the BAND package, version 2022.101,⁵⁵ was used on the VASP geometries of hydrogen *Cmca-4*, optimized with the PBE and the R²SCAN functionals at 700 GPa. Scalar relativistic effects were included using the Zero Order Regular Approximation (ZORA).⁵⁶ A double- ζ polarized (DZP) basis set was used for this calculation.⁵⁷ The integration quality was kept equal to 'Very Good' for all calculations.

References

- (1) Wigner, E.; Huntington, H. B. On the Possibility of a Metallic Modification of Hydrogen. *J. Chem. Phys.* **1935**, 3 (12), 764–770. <https://doi.org/10.1063/1.1749590>.
- (2) Zaghou, M.; Salamat, A.; Silvera, I. F. Evidence of a First-Order Phase Transition to Metallic Hydrogen. *Phys. Rev. B* **2016**, 93, 155128. <https://doi.org/10.1103/PhysRevB.93.155128>.
- (3) Silvera, I. F.; Dias, R. Metallic Hydrogen. *J. Phys. Condens. Matter* **2018**, 30, 254003.

https://doi.org/10.1088/1361-648X/aac401.

(4) McMahon, J. M.; Ceperley, D. M. Ground-State Structures of Atomic Metallic Hydrogen. *Phys. Rev. Lett.* **2011**, *106*, 165302. https://doi.org/10.1103/PhysRevLett.106.165302.

(5) Loubeyre, P.; Occelli, F.; Dumas, P. Synchrotron Infrared Spectroscopic Evidence of the Probable Transition to Metal Hydrogen. *Nature* **2020**, *577* (7792), 631–635. https://doi.org/10.1038/s41586-019-1927-3.

(6) Eremets, M. I.; Drozdov, A. P.; Kong, P. P.; Wang, H. Semimetallic Molecular Hydrogen at Pressure above 350 GPa. *Nat. Phys.* **2019**, *15* (12), 1246–1249. https://doi.org/10.1038/s41567-019-0646-x.

(7) Dewaele, A.; Loubeyre, P.; Occelli, F.; Marie, O.; Mezouar, M. Toroidal Diamond Anvil Cell for Detailed Measurements under Extreme Static Pressures. *Nat. Commun.* **2018**, *9*, 2913. https://doi.org/10.1038/s41467-018-05294-2.

(8) Ji, C.; Li, B.; Luo, J.; Zhao, Y.; Liu, Y.; Glazyrin, K. Ultrahigh-Pressure Crystallographic Passage towards Metallic Hydrogen. *Nature* **2025**. https://doi.org/10.1038/s41586-025-08936-w.

(9) Perdew, J. P.; Zunger, A. Self-Interaction Correction to Density-Functional Approximations for Many-Electron Systems. *Phys. Rev. B* **1981**, *23* (10), 5048–5079. https://doi.org/10.1103/PhysRevB.23.5048.

(10) Cohen, A. J.; Mori-Sánchez, P.; Yang, W. Insights into Current Limitations of Density Functional Theory. *Science (80-).* **2008**, *321* (5890), 792–794. https://doi.org/10.1126/science.1158722.

(11) Schmidt, T.; Kraisler, E.; Kronik, L.; Kümmel, S. One-Electron Self-Interaction and the Asymptotics of the Kohn-Sham Potential: An Impaired Relation. *Phys. Chem. Chem. Phys.* **2014**, *16* (28), 14357–14367. https://doi.org/10.1039/c3cp55433c.

(12) Gritsenko, O. V.; Braïda, B.; Baerends, E. J. Physical Interpretation and Evaluation of the Kohn-Sham and Dyson Components of the ϵ - I Relations between the Kohn-Sham Orbital Energies and the Ionization Potentials. *J. Chem. Phys.* **2003**, *119* (4), 1937–1950. https://doi.org/10.1063/1.1582839.

(13) Perdew, J. P.; Burke, K.; Ernzerhof, M. Generalized Gradient Approximation Made Simple. *Phys. Rev. Lett.* **1996**, *77* (18), 3865–3868. https://doi.org/10.1103/PhysRevLett.77.3865.

(14) Racioppi, S.; Lolur, P.; Hyldgaard, P.; Rahm, M. A Density Functional Theory for the Average Electron Energy. *J. Chem. Theory Comput.* **2023**, *19*, 799–807. https://doi.org/10.1021/acs.jctc.2c00899.

(15) Perdew, J. P.; Ruzsinszky, A.; Constantin, L. A.; Sun, J.; Csonka, G. I. Some Fundamental Issues in Ground-State Density Functional Theory: A Guide for the Perplexed. *J. Chem. Theory Comput.* **2009**, *5* (4), 902–908. https://doi.org/10.1021/ct800531s.

(16) Tao, J.; Perdew, J. P.; Staroverov, V. N.; Scuseria, G. E. Climbing the Density Functional Ladder: Nonempirical Meta-Generalized Gradient Approximation Designed for Molecules and Solids. *Phys. Rev. Lett.* **2003**, *91* (14), 146401. https://doi.org/10.1103/PhysRevLett.91.146401.

(17) Staroverov, V. N.; Scuseria, G. E.; Tao, J.; Perdew, J. P. Tests of a Ladder of Density Functionals for Bulk Solids and Surfaces. *Phys. Rev. B - Condens. Matter Mater. Phys.* **2004**, *69* (7), 1–11. https://doi.org/10.1103/PhysRevB.69.075102.

(18) Perdew, J. P.; Staroverov, V. N.; Tao, J.; Scuseria, G. E. Density Functional with Full Exact Exchange, Balanced Nonlocality of Correlation, and Constraint Satisfaction. *Phys. Rev. A - At. Mol. Opt. Phys.* **2008**, *78* (5), 052513. https://doi.org/10.1103/PhysRevA.78.052513.

(19) Yang, Z. H.; Peng, H.; Sun, J.; Perdew, J. P. More Realistic Band Gaps from Meta-Generalized Gradient Approximations: Only in a Generalized Kohn-Sham Scheme. *Phys. Rev. B* **2016**, *93*, 205205. https://doi.org/10.1103/PhysRevB.93.205205.

(20) Lebeda, T.; Aschebrock, T.; Sun, J.; Leppert, L.; Kümmel, S. Right Band Gaps for the Right Reason at Low Computational Cost with a Meta-GGA. *Phys. Rev. Mater.* **2023**, *7*, 093830. https://doi.org/10.1103/PhysRevMaterials.7.093803.

(21) Bonitz, M.; Vorberger, J.; Bethkenhagen, M.; Böhme, M.; Ceperley, D.; Filinov, A.; Gawne, T.; Graziani, F.; Gregori, G.; Hamann, P.; Hansen, S.; Holzmann, M.; Hu, S. X.; Kählert, H.; Karasiev, V.; Kleinschmidt, U.; Kordts, L.; Makait, C.; Militzer, B.; Moldabekov, Z.; Pierleoni, C.; Preising, M.; Ramakrishna, K.; Redmer, R.; Schwalbe, S.; Svensson, P.; Dornheim, T. First Principles Simulations of Dense Hydrogen. *Comput. Phys.* **2024**, 1–105.

(22) Liao, K.; Li, X. Z.; Alavi, A.; Grüneis, A. A Comparative Study Using State-of-the-Art Electronic Structure Theories on Solid Hydrogen Phases under High Pressures. *npj Comput. Mater.* **2019**, *5*,

100. <https://doi.org/10.1038/s41524-019-0243-7>.

(23) Mejía-Rodríguez, D.; Trickey, S. B. Meta-GGA Performance in Solids at Almost GGA Cost. *Phys. Rev. B - Condens. Matter Mater. Phys.* **2020**, *102*, 121109(R).
<https://doi.org/10.1103/PhysRevB.102.121109>.

(24) Furness, J. W.; Kaplan, A. D.; Ning, J.; Perdew, J. P.; Sun, J. Accurate and Numerically Efficient R2SCAN Meta-Generalized Gradient Approximation. *J. Phys. Chem. Lett.* **2020**, *11* (19), 8208–8215. <https://doi.org/10.1021/acs.jpclett.0c02405>.

(25) Pickard, C. J.; Needs, R. J. Structure of Phase III of Solid Hydrogen. *Nat. Phys.* **2007**, *3* (7), 473–476. <https://doi.org/10.1038/nphys625>.

(26) Edwards, B.; Ashcroft, N. W.; Lenosky, T. Layering Transitions and the Structure of Dense Hydrogen. *Europhys. Lett.* **1996**, *34* (7), 519–524. <https://doi.org/10.1209/epl/i1996-00489-5>.

(27) Borinaga, M.; Riego, P.; Leonardo, A.; Calandra, M.; Mauri, F.; Bergara, A.; Errea, I. Anharmonic Enhancement of Superconductivity in Metallic Molecular Cmca - 4 Hydrogen at High Pressure: A First-Principles Study. *J. Phys. Condens. Matter* **2016**, *28*, 494001. <https://doi.org/10.1088/0953-8984/28/49/494001>.

(28) Monacelli, L.; Casula, M.; Nakano, K.; Sorella, S.; Mauri, F. Quantum Phase Diagram of High-Pressure Hydrogen. *Nat. Phys.* **2023**, *19* (6), 845–850. <https://doi.org/10.1038/s41567-023-01960-5>.

(29) Nagao, K.; Nagara, H.; Matsubara, S. Structures of Hydrogen at Megabar Pressures. *Phys. Rev. B - Condens. Matter Mater. Phys.* **1997**, *56* (5), 2295–2298.
<https://doi.org/10.1103/PhysRevB.56.2295>.

(30) Azadi, S.; Monserrat, B.; Foulkes, W. M. C.; Needs, R. J. Dissociation of High-P Ressure Solid Molecular Hydrogen: A Quantum Monte Carlo and Anharmonic Vibrational Study. *Phys. Rev. Lett.* **2014**, *112*, 165501. <https://doi.org/10.1103/PhysRevLett.112.165501>.

(31) Needs, R. J.; Towler, M. D.; Drummond, N. D.; López Ríos, P. Continuum Variational and Diffusion Quantum Monte Carlo Calculations. *J. Phys. Condens. Matter* **2010**, *22*, 023201.
<https://doi.org/10.1088/0953-8984/22/2/023201>.

(32) Grossman, J. C. Benchmark Quantum Monte Carlo Calculations. *J. Chem. Phys.* **2002**, *117* (4), 1434–1440. <https://doi.org/10.1063/1.1487829>.

(33) McMinis, J.; Clay, R. C.; Lee, D.; Morales, M. A. Molecular to Atomic Phase Transition in Hydrogen under High Pressure. *Phys. Rev. Lett.* **2015**, *114*, 105305.
<https://doi.org/10.1103/PhysRevLett.114.105305>.

(34) Hui, K.; Chai, J. Da. SCAN-Based Hybrid and Double-Hybrid Density Functionals from Models without Fitted Parameters. *J. Chem. Phys.* **2016**, *144*, 044114. <https://doi.org/10.1063/1.4940734>.

(35) Cheng, B.; Bethkenhagen, M.; Pickard, C. J.; Hamel, S. Phase Behaviours of Superionic Water at Planetary Conditions. *Nat. Phys.* **2021**, *17* (11), 1228–1232. <https://doi.org/10.1038/s41567-021-01334-9>.

(36) Errea, I.; Belli, F.; Monacelli, L.; Sanna, A.; Koretsune, T.; Tadano, T.; Bianco, R.; Calandra, M.; Arita, R.; Mauri, F.; Flores-Livas, J. A. Quantum Crystal Structure in the 250-Kelvin Superconducting Lanthanum Hydride. *Nature* **2020**, *578* (7793), 66–69.
<https://doi.org/10.1038/s41586-020-1955-z>.

(37) Dangić, Đ.; Monacelli, L.; Bianco, R.; Mauri, F.; Errea, I. Large Impact of Phonon Lineshapes on the Superconductivity of Solid Hydrogen. *Commun. Phys.* **2024**, *7*, 150.
<https://doi.org/10.1038/s42005-024-01643-4>.

(38) Monacelli, L.; Bianco, R.; Cherubini, M.; Calandra, M.; Errea, I.; Mauri, F. The Stochastic Self-Consistent Harmonic Approximation: Calculating Vibrational Properties of Materials with Full Quantum and Anharmonic Effects. *J. Phys. Condens. Matter* **2021**, *33*, 363001.
<https://doi.org/10.1088/1361-648X/ac066b>.

(39) Borinaga, M.; Errea, I.; Calandra, M.; Mauri, F.; Bergara, A. Anharmonic Effects in Atomic Hydrogen: Superconductivity and Lattice Dynamical Stability. *Phys. Rev. B* **2016**, *93*, 174308.
<https://doi.org/10.1103/PhysRevB.93.174308>.

(40) Raupach, M.; Tonner, R. A Periodic Energy Decomposition Analysis Method for the Investigation of Chemical Bonding in Extended Systems. *J. Chem. Phys.* **2015**, *142*, 194105.
<https://doi.org/10.1063/1.4919943>.

(41) Lonie, D. C.; Zurek, E. XtalOpt: An Open-Source Evolutionary Algorithm for Crystal Structure Prediction. *Comput. Phys. Commun.* **2011**, *182* (2), 372–387.

https://doi.org/10.1016/j.cpc.2010.07.048.

(42) Hajinazar, S.; Zurek, E. XtalOpt Version 13: Multi-Objective Evolutionary Search for Novel Functional Materials. *Comput. Phys. Commun.* **2024**, *304*, 109306.

(43) Avery, P.; Zurek, E. RandSpg: An Open-Source Program for Generating Atomistic Crystal Structures with Specific Spacegroups. *Comput. Phys. Commun.* **2017**, *213*, 208–216. https://doi.org/10.1016/j.cpc.2016.12.005.

(44) Lonie, D. C.; Zurek, E. Identifying Duplicate Crystal Structures: XtalComp, an Open-Source Solution. *Comput. Phys. Commun.* **2012**, *183* (3), 690–697. https://doi.org/10.1016/j.cpc.2011.11.007.

(45) Kresse, G.; Hafner, J. Ab Initio Molecular-Dynamics Simulation of the Liquid-Metalamorphous-Semiconductor Transition in Germanium. *Phys. Rev. B* **1994**, *49* (20), 14251–14269. https://doi.org/10.1103/PhysRevB.49.14251.

(46) Blöchl, P. E. Projector Augmented-Wave Method. *Phys. Rev. B - Condens. Matter Mater. Phys.* **1994**, *50* (24), 17953–17979. https://doi.org/10.1103/PhysRevB.50.17953.

(47) Monkhorst, H. J.; Pack, J. D. Special Points for Brillouin-Zone Integrations. *Phys. Rev. B - Condens. Matter Mater. Phys.* **1976**, *13* (12), 5188–5192. https://doi.org/10.1103/PhysRevB.16.1748.

(48) Methfessel, M.; Paxton, A. T. High-Precision Sampling for Brillouin-Zone Integration in Metals. *Phys. Rev. B* **1989**, *40* (6), 3616–3621. https://doi.org/10.1103/PhysRevB.40.3616.

(49) Blöchl, P. E.; Jepsen, O.; Andersen, O. K. Improved Tetrahedron Method for the Brillouin-Zone Integrations. *Phys. Rev. B* **1994**, *49* (23), 16223–16233.

(50) Bader, R. F. W. *Atoms in Molecules: A Quantum Theory*, International Series of Monographs on Chemistry; Oxford: Oxford Science Publications, 1990; Vol. 22.

(51) Otero-De-La-Roza, A.; Johnson, E. R.; Luña, V. Critic2: A Program for Real-Space Analysis of Quantum Chemical Interactions in Solids. *Comput. Phys. Commun.* **2014**, *185* (3), 1007–1018. https://doi.org/10.1016/j.cpc.2013.10.026.

(52) Togo, A.; Oba, F.; Tanaka, I. First-Principles Calculations of the Ferroelastic Transition between Rutile-Type and CaCl₂-Type SiO₂ at High Pressures. *Phys. Rev. B - Condens. Matter Mater. Phys.* **2008**, *78*, 134106. https://doi.org/10.1103/PhysRevB.78.134106.

(53) Hoover, W. G.; Ladd, A. J. C.; Moran, B. High-Strain-Rate Plastic Flow Studied via Nonequilibrium Molecular Dynamics. *Phys. Rev. Lett.* **1982**, *48* (26), 1818–1820. https://doi.org/10.1103/PhysRevLett.48.1818.

(54) Evans, D. J. Computer “Experiment” for Nonlinear Thermodynamics of Couette Flow. *J. Chem. Phys.* **1983**, *78* (6), 3297–3302. https://doi.org/10.1063/1.445195.

(55) Philipsen, P. H. T.; Velde, G. te; Baerends, E. J.; Berger, J. A.; Boeij, P. L. de; Franchini, M.; Groeneveld, J. A.; Kadantsev, E. S.; Klooster, R.; Kootstra, F.; M.C.W.M. Pols, P. R.; Raupach, M.; Skachkov, D. G.; Snijders, J. G.; Verzijl, C. J. O.; Gil, J. A. C.; Thijssen, J. M.; Wiesenecker, G.; Peeples, C. A.; Schreckenbach, G.; Ziegler, T. BAND 2022.101, SCM, Theoretical Chemistry, Vrije Universiteit, Amsterdam, The Netherlands, [Http://Www.Scm.Com](http://Www.Scm.Com). **2022**.

(56) Philipsen, P.; van Lenthe, E.; Snijders, J.; Baerends, E. Relativistic Calculations on the Adsorption of CO on the (111) Surfaces of Ni, Pd, and Pt within the Zeroth-Order Regular Approximation. *Phys. Rev. B - Condens. Matter Mater. Phys.* **1997**, *56* (20), 13556–13562. https://doi.org/10.1103/PhysRevB.56.13556.

(57) Kadantsev, E. S.; Klooster, R.; De Boeij, P. L.; Ziegler, T. The Formulation and Implementation of Analytic Energy Gradients for Periodic Density Functional Calculations with STO/NAO Bloch Basis Set. *Mol. Phys.* **2007**, *105* (19–22), 2583–2596. https://doi.org/10.1080/00268970701598063.

(58) *International Tables for Crystallography Volume A: Space-Group Symmetry*, Second.; M. I. Aroyo, Ed.; 2016. https://doi.org/10.1107/97809553602060000114.

(59) Koritsanszky, T. S.; Coppens, P. Chemical Applications of X-Ray Charge-Density Analysis. *Chem. Rev.* **2001**, *101*, 1583–1627.

(60) Gatti, C. Chemical Bonding in Crystals: New Directions. *Zeitschrift fur Krist.* **2005**, *220* (5–6), 399–457. https://doi.org/10.1524/zkri.220.5.399.65073.

(61) Della Pergola, R.; Sironi, A.; Colombo, V.; Garlaschelli, L.; Racioppi, S.; Sironi, A.; Macchi, P. Periodical Trends in [Co₆E(CO)₁₆]- Clusters: Structural, Synthetic and Energy Changes Produced by Substitution of P with As. *J. Organomet. Chem.* **2017**, *849–850*, 130–136. https://doi.org/10.1016/j.jorgancchem.2017.05.041.

(62) Abramov, Y. A. On the Possibility of Kinetic Energy Density Evaluation from the Experimental Electron-Density Distribution. *Acta Crystallogr. Sect. A Found. Crystallogr.* **1997**, *53* (3), 264–272. <https://doi.org/10.1107/S010876739601495X>.

(63) Espinosa, E.; Alkorta, I.; Rozas, I.; Elguero, J.; Molins, E. About the Evaluation of the Local Kinetic, Potential and Total Energy Densities in Closed-Shell Interactions. *Chem. Phys. Lett.* **2001**, *336* (5–6), 457–461. [https://doi.org/10.1016/S0009-2614\(01\)00178-6](https://doi.org/10.1016/S0009-2614(01)00178-6).

(64) Espinosa, E.; Alkorta, I.; Elguero, J.; Molins, E. From Weak to Strong Interactions: A Comprehensive Analysis of the Topological and Energetic Properties of the Electron Density Distribution Involving X-H···F-Y Systems. *J. Chem. Phys.* **2002**, *117* (12), 5529–5542. <https://doi.org/10.1063/1.1501133>.

(65) Zhao, L.; Hopffgarten, M. von; Andrada, D. M.; Frenking, G. Energy Decomposition Analysis. *Wiley Interdiscip. Rev. Comput. Mol. Sci.* **2018**, *8*, e1345. <https://doi.org/10.1002/wcms.1345>.

Supplementary Information

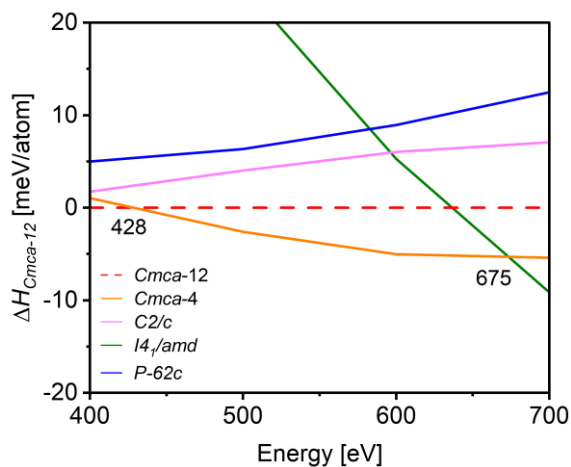


Figure S1. Enthalpy differences ($\Delta H = \Delta E + P\Delta V$) as a function of pressure for the high-pressure phases of hydrogen calculated with VASP using the meta-GGA exchange-correlation functional R²SCAN, between 400 GPa and 700 GPa. The transition pressures are marked at 428 and 675 GPa. Notice that the previously reported $P6_2/c$ structure,²⁸ refers in reality to the $P-62c$ space group, since $P6_2/c$ does not exist as a space group.⁵⁸

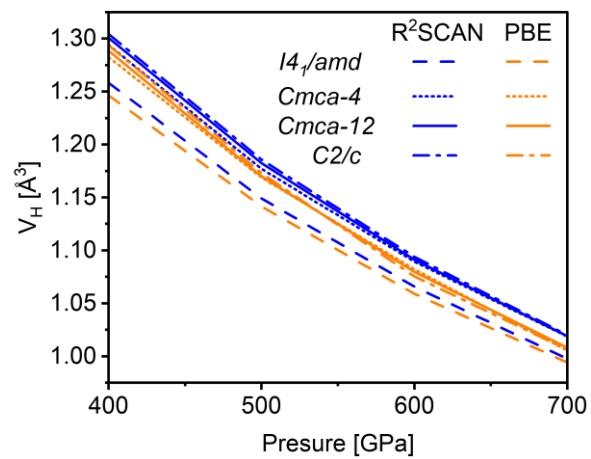


Figure S2. Atomic volumes per hydrogen in function of pressure, calculated with VASP using the PBE and the R²SCAN functionals.

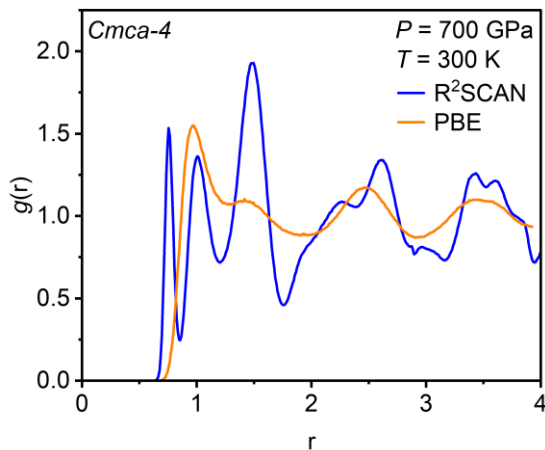


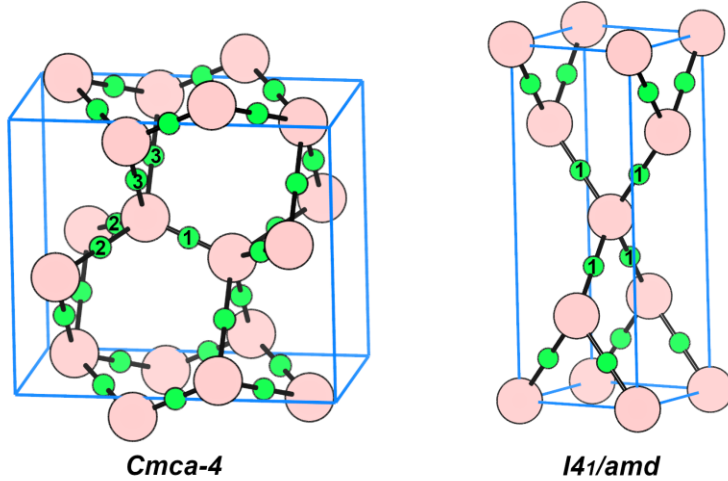
Figure S3. Pair distribution function $g(r)$ calculated in NPT molecular dynamics of *Cmca-4* at $T=300$ K and $P = 700$ GPa with R^2 SCAN (blue line) and PBE (orange line). The $g(r)$ profile calculated with meta-GGA functional is that of a crystalline phase, while the one calculated with the GGA functional is that of a liquid phase.

Overview on the Quantum Theory of Atoms in Molecules (QTAIM).

The QTAIM is the cornerstone method to study chemical bonding in real space, both from theoretical and experimental data.^{59,60} QTAIM studies the local topological features of the electron density, $\rho(\mathbf{r})$, mapping critical points and evaluating chemical bonding and properties based on $\rho(\mathbf{r})$.

The bond critical points (bcp), in particular, are special points in the electron density where $\nabla\rho(\mathbf{r}) = 0$, and are associated with the presence of bonding interactions between atoms.⁶⁰ The amount of electron density at the point $\rho(\mathbf{r})$ gives estimates on the interaction's strength between two atoms.⁶¹ The Laplacian of the electron density $\nabla^2\rho(\mathbf{r})$ quantifies the degree of localization and curvature of the electron density at the bcp. Generally, large and negative values of $\nabla^2\rho(\mathbf{r})$ correspond to covalent interactions, while $\nabla^2\rho(\mathbf{r}) > 0$ is found in hydrogen-bonds or van der Waals interactions. The bond ellipticity ϵ , is related to the deviation of charge distribution from cylindrical symmetry (σ -type of interaction) at bcp. Values of $\epsilon \sim 0$ correspond interactions having cylindrical symmetry.

The total energy density at the bcp, named H , is the sum of $G + V$, the kinetic energy and the potential energy densities at the bcp. The more negative the H , the stronger the interaction. The kinetic energy density G is evaluated following the Abramov approximation.^{62,63} The potential energy density at the bcp is then calculated using the local form of the virial theorem, $2G + V = 1/4\nabla^2\rho(\mathbf{r})$, which will consequently be negative. The ratio $|V|/G$, is useful to characterize the type of interaction at the bcp.^{60,64} A ratio $|V|/G < 1$ corresponds to a closed-shell interaction region (ionic), while $|V|/G > 2$ corresponds to a shared-shell interaction region, such as covalent bonds. Values between $1 < |V|/G < 2$ are the intermediate regions.⁶⁰

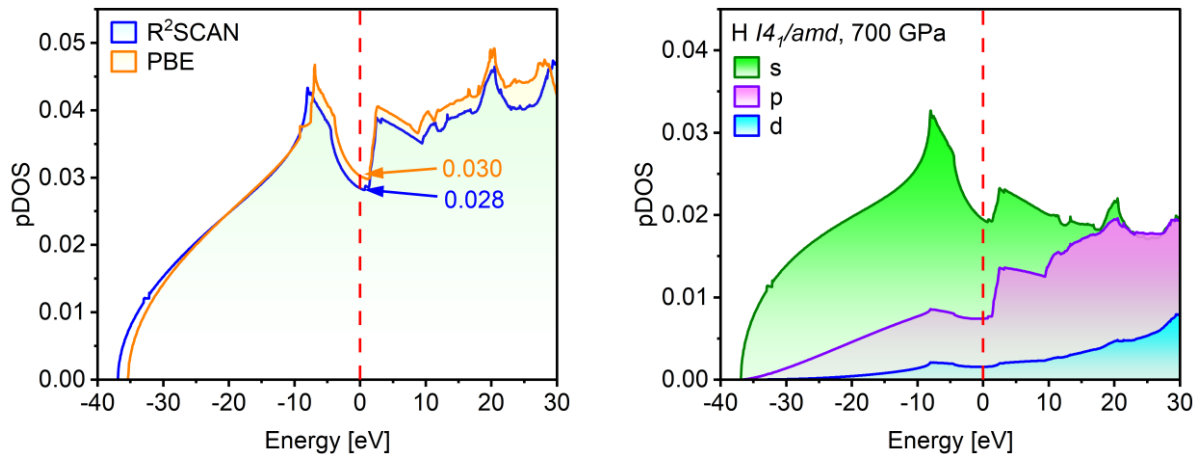


R²SCAN / PBE

<i>Cmca-4</i>	$\rho(r)$	$\nabla^2\rho(r)$	ϵ	$-H$	$ V /G$
1	0.301 / 0.232	-1.213 / -0.346	0.076 / 0.206	0.490 / 0.281	3.621 / 2.447
2	0.161 / 0.189	0.169 / 0.073	0.178 / 0.294	0.122 / 0.173	1.743 / 1.905
3	0.131 / 0.127	0.240 / 0.280	0.067 / 0.982	0.076 / 0.069	1.560 / 1.496

<i>I4₁/amd</i>	$\rho(r)$	$\nabla^2\rho(r)$	ϵ	$-H$	$ V /G$
1	0.183 / 0.180	0.022 / 0.036	0.746 / 0.758	0.168 / 0.162	1.968 / 1.947

Figure S4. (Top) Crystal structures of *Cmca-4* and *I4₁/amd* in their conventional unit cells. The green spheres mark the topological bond critical points, which are numerated in accordance to the table below. (Bottom) Topological descriptors calculated using the QTAIM. $\rho(r)$: electron density at the bcp [e/bohr³]; $\nabla^2\rho(r)$: Laplacian of the electron density at the bcp [e/bohr⁵]; ϵ : bond ellipticity; $-H$: total energy density at the bcp taken with the negative value [hartree/bohr³]; $|V_b|/G_b$: potential/kinetic energy density ratio.⁶⁰



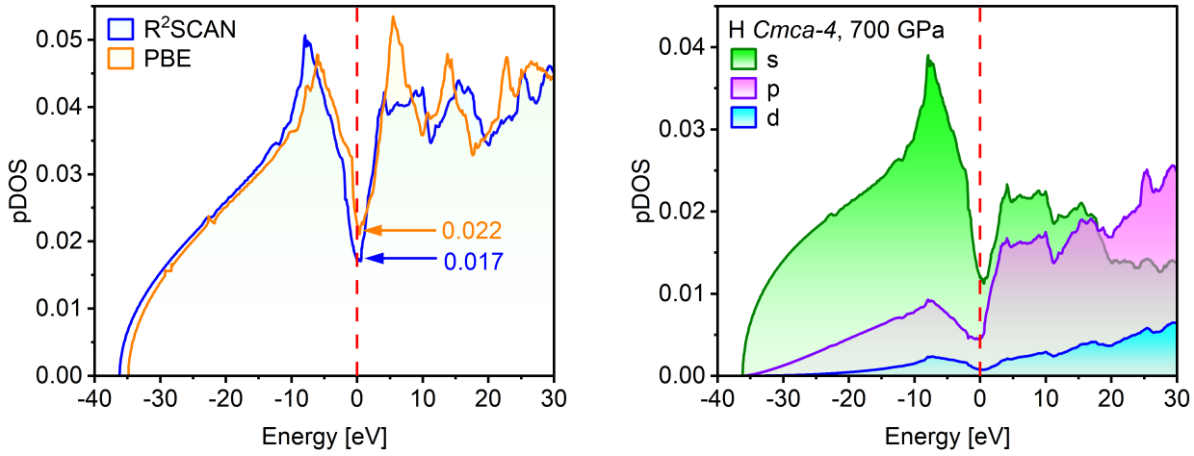


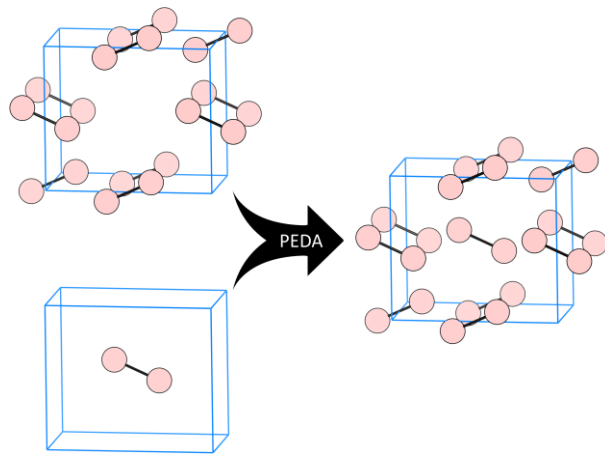
Figure S5. (Left) Total density of states (DOS) calculated for *I4₁/amd* and *Cmca-4* at 700 GPa with VASP using the PBE and the R²SCAN functionals. The values of the density of states at the Fermi level ($g(E_F)$) are reported. The value of DOS at $g(E_F)$ calculated with PBE for the atomic phase is only 7% higher compared to the one calculated at the meta-GGA level of theory. On the other hand, for the molecular phase *Cmca-4*, the DOS at $g(E_F)$ calculated with PBE is almost 30% higher than R²SCAN. (Right) Projected density of states (pDOS) calculated for *I4₁/amd*, *Cmca-4* at 700 GPa with VASP using the R²SCAN functionals.

Periodic Energy Decomposition Analysis (PEDA)

To better understand the character of the intermolecular interactions between a molecule of H₂ in *Cmca-4* with the rest of the crystal, we performed an energy decomposition analysis (EDA) using the Ziegler-Rauk variant,⁶⁵ which decomposes the total interaction energy (ΔE_{int}) between two prepared fragments into chemically meaningful terms. The term “prepared” means that the atoms in the moieties that are compared possess the same local coordinates as in the final product (Figure S6). Notice that all the interaction energies, ΔE_{int} , are positive, since they account only for the electronic energy associated with the reaction (they do not consider the *PV* contribution).

In EDA, the total interaction energy, ΔE_{int} , is decomposed into a Pauli repulsion energy, ΔE_{Pauli} , which is usually destabilizing; an electrostatic term, ΔE_{Elec} , which can quantify the ionic character of an interaction, and finally an orbital term, ΔE_{Orb} , which accounts for the covalent character of the total interaction. Often, the Pauli repulsion energy and the electrostatic energy are coupled together in a term named the steric interactions, ΔE_{Steric} , which combines all the charge-charge components in a chemically intuitive term.

The total interaction energy, ΔE_{int} , calculated by EDA should not be confused with the ΔE term in the calculation of the enthalpy of formation, ΔH . In the first case, the electronic energy of interaction is evaluated upon the reaction between two moieties possessing the same geometry as in the final product. In the second, ΔH is evaluated from the isolated reactants at their ground states, which is composed by the thermodynamic terms ΔE and $P\Delta V$.



Terms	PBE	$R^2\text{SCAN}_{\text{PBE}}$	$R^2\text{SCAN}$
ΔE_{Pauli}	59.931	60.136	46.435
ΔE_{elstat}	-9.929	-9.732	-8.274
ΔE_{orb}	-42.157	-42.541	-30.076
ΔE_{int}	7.846	7.863	8.085

Figure S6. (Left) Scheme of the energy decomposition analysis. (Right) PEDa energy terms. PBE = PBE calculation on the PBE optimized structure at 700 GPa; $R^2\text{SCAN}_{\text{PBE}}$ = $R^2\text{SCAN}$ calculation on the PBE optimized structure at 700 GPa; $R^2\text{SCAN}$ = $R^2\text{SCAN}$ calculation on the $R^2\text{SCAN}$ optimized structure at 700 GPa.